JCTC Journal of Chemical Theory and Computation

pubs.acs.org/JCTC Article

Routes of Transport in the Path Integral Lindblad Dynamics through State-to-State Analysis

Devansh Sharma and Amartya Bose*

Cite This: J. Chem. Theory Comput. 2026, 22, 3827−3838 Read Online

ACCESS | Metrics & More | Article Recommendations

ABSTRACT: Analyzing routes of transport for open quantum systems with nonequilibrium initial conditions, such as exciton transport aggregates, is extremely challenging. The state-to-state approach [A. Bose, and P. L. Walters, J. Chem. Theory Comput. 2023, **19**, 15, 4828−4836] has proven to be a useful method for understanding transport mechanisms in quantum systems interacting with dissipative thermal baths. However, real systems are often exposed to processes that may lead to either increase or decrease of the number of excitations in the aggregate. Such pumping or draining processes can also affect the routes of transport. We extend the state-to-state analysis to account for approximate Lindbladian descriptions of generic dissipative, pumping and decohering processes acting on a system, which is exchanging energy with a thermal bath. The exchange of energy between the system and the environment is incorporated in a numerically exact manner. This Lindblad state-to-state analysis framework is able to unravel the internal transport pathways along with the effect of the external empirical processes and how the thermal solvents modulate these transport routes. Using this new state-to-state formalism, we demonstrate different mechanistic aspects, including the establishment of steady-state excitonic currents in molecular aggregates under the simultaneous influence of pumps and drains whose dynamics is simulated using the path integral Lindblad dynamics [A. Bose, J. Phys. Chem. Lett. 2024, **15**, 12, 3363−3368]. It is especially lucrative that in the absence of such processes, the current method reduces to the standard state-to-state approach. We believe that this Lindblad state-to-state method promises to be a unique tool for understanding the dynamics of open quantum systems subject to a host of additional processes with unprecedented granularity, enabling unique questions to be asked about these systems of great complexity.

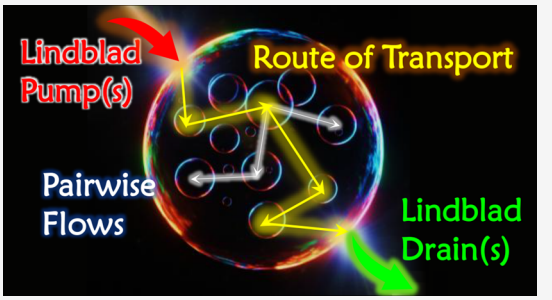

1. INTRODUCTION

Transport processes are ubiquitous. Be it the exciton transport in light-harvesting antenna complexes in photosynthetic systems[1−4] or the charge transport in molecular wires and solar cells,[5,6] transport plays a pivotal role in their functioning. Simulating and understanding such processes is instrumental for getting insights into the functioning of various molecular systems as well as ideas for designing new materials. However, these simulations involving quantum particles in condensed phases are complicated. Tackling the already large number of electronic degrees of freedom of complex aggregates, which is what such transport systems generally are, along with a plethora of environmental modes with limited computational resources and time, requires some thought. Over the years, methods that simulate the reduced density matrix (RDM) of the system, either in a numerically exact[7−14] or approximate manner,[15−19] have been the methods of choice when it comes to simulating the nonequilibrium dynamics at a nonzero temperature.

However, in addition to the complexity of simulating the dynamics of these condensed phase systems, another concern that has started to receive some attention of late is the question of routes of transport. Traditional numerical simulations simply yield the reduced density matrix of the system as a function of time. The subsequent quest, therefore, is one of gaining mechanistic insight into the transport that happens. Various methods have been developed that all stem from the idea of population fluxes. Initial ideas of using flux-balance and flux networks have been used in this context for understanding transport in light-harvesting Fenna−Matthews−Olson (FMO) complex.[2] More recently, Dani and Makri[20] have tried to understand the concept of coherence maps as they relate to the system dynamics. One of us has developed the related idea of state-to-state transport[21,22] which can unravel the initial condition-dependent dynamical pathways that are present in the system in a mathematically rigorous manner. This state-to-state approach decomposes the dynamics into direct unmediated transport flows between any two sites in the

Received: January 7, 2026
Revised: March 16, 2026
Accepted: March 20, 2026
Published: April 6, 2026

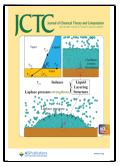

presence of thermal baths, thereby allowing us to identify the important connections in a dynamical manner, and follow the quantum particle as it moves from one site to another over time. These pairwise flows can then be pieced together to determine the routes of transport.

Most of the quantum and semiclassical methods described, and the methods of analyzing routes of transport deal with systems that are closed in terms of particle-number.[23−27] This has serious consequences for the dynamics. For instance in various photosynthetic light-harvesting systems, there is typically a sink site that funnels the excitation into a "special-pair" of chlorophyll molecules, which further channels it into the reaction center. Now, typically, in simulations of the light-harvesting antenna complexes of photosynthesis, the attention is on the transport of the excitation before it gets harvested. Consequently, they ignore the special pair and reaction center, which while improving the numerical efficiency of the simulations, leads to a buildup of excitation population on these sink sites. Not only is this build-up not physical, if the extraction is accounted for, the details of the transport may change owing to the many-body nature and mechanism of dynamics.

It is often computationally convenient to deal with processes like the extraction of excitation as discussed in an empirical way. The effect of these empirical processes happen on top of how the system and the solvent environment interact. Using non-Hermitian systems with QuAPI[28] is one way of incorporating particle loss in a system empirically. We have extended our state-to-state analysis[21] to the study the routes of transport for such non-Hermitian quantum systems interacting with a thermal solvent environment.[29] However, there are severe limitations to the sort of processes that can be treated using non-Hermitian systems. The non-Hermiticity makes the time-evolution nonunitary violating the completely positive and trace-preserving (CPTP) nature of the density matrix evolution. Additionally, while non-Hermitian descriptions may be enough for dealing with systems with empirical drains, this formalism cannot describe systems that are pumped. In fact, there are a multitude of other processes, like spin dephasing, that if treated empirically cannot be described by non-Hermitian Hamiltonians. To handle both these issues, we have recently introduced the path integral Lindblad method of dynamics[30] (PILD) which combines Feynman-Vernon path integral[31] description of the system interacting with a thermal solvent environment with a Lindblad master equation[32,33] description of the empirical processes. A combination of semiclassical dynamics and Lindblad master equations has recently been used for investigating 2D spectra of exciton-polaritons in the presence of cavity losses.[34]

In this paper, we extend the state-to-state analysis[21,29] to analyze the routes of transport in systems subject to the simultaneous influence of solvent environments, expressed as baths, and empirical processes encoded approximately through Lindblad jump operators. In a sense, the present Lindblad state-to-state method describes a formalism that accounts for a superset of physical phenomena including pump processes in comparison to the previous non-Hermitian idea.[29] Consistent with other developments of the state-to-state method, our Lindblad state-to-state is similarly independent of the exact method used to simulate the dynamics of the system RDM so long as the impacts of both the thermal bath and the Lindblad empirical processes are incorporated. PILD[30] is one of the many methods that can be used for simulating the time-evolved RDM. An interesting side-result of the derivation of the method is that though the RDM of the system itself satisfies a non-Markovian equation of motion that incorporates both the memory kernel induced by the solvent environment and the Markovian terms corresponding to the Lindblad master equation, the state-to-state analysis does not require the explicit calculation of the memory kernel and can be obtained directly from the time-evolved system RDM, the system Hamiltonian and the Lindblad jump operators.

We start by developing the method in Section 2, following which in Section 3.1, we demonstrate its validity through a consistency check with the previous non-Hermitian method for the case of an exciton-polariton system with two competing loss mechanisms. We then apply the new method to explore systems involving both pumps and drains (Sections 3.2 and 3.3). We show how the flows between monomers happen in the presence of both pumps and drains, leading to steady state excitonic currents being set up in the aggregates. The time-evolved RDMs that are used for the current state-to-state Lindblad analysis were run with the non-Markovian path integral Lindblad dynamics method[30] in all of these cases. Finally, we end with some concluding remarks in Section 4. Additionally, a discussion on the differences between a non-Hermitian description and the Lindblad formalism is presented in Appendix A. An alternative derivation of the current state-to-state method manifestly demonstrating that the memory kernel does not explicitly appear in the state-to-state formulas is shown in Appendix B.

2. METHOD

Consider a N-state system coupled to a solvent environment that, under Gaussian response theory, has been mapped onto harmonic bath(s):

$$\hat{H} = \hat{H}_{\text{sys}} + \hat{H}_{\text{bath}} + \hat{H}_{\text{sys-bath}} \tag{1}$$

where we assume there are N_b independent baths of harmonic oscillators:

$$\hat{H}_{\text{bath}} = \sum_{s=1}^{N_b} \sum_{b} \frac{p_{sb}^2}{2} + \frac{1}{2}\omega_{sb}^2 x_{sb}^2 \tag{2}$$

$$\hat{H}_{\text{sys-bath}} = -\sum_{s=1}^{N_b} \sum_{b} c_{sb} x_{sb} \hat{S}_s \tag{3}$$

where the jth bath interacts with the system through the operator $\hat{S}_j$ and is characterized by the spectral density,

$$J_j(\omega) = \frac{\pi}{2} \sum_{b} \frac{c_{jb}^2}{\omega_{jb}} \delta(\omega - \omega_{jb}) \tag{4}$$

obtained from molecular dynamics simulations or directly from experiments. Often, for charge and exciton transport where the electronic states form the system, nuclear motions of the molecules that are a part of the system and those that are a part of the solvent both contribute to the bath degrees of freedom. Simulations of the dynamics of this system-bath couple (eq 1) scales exponentially with the dimensionality of the full Hilbert space, and consequently becomes intractable. Therefore, simulations are done for the reduced density matrix corresponding to the system, $\rho_{\text{sys}}(t)$.

Methods based on Feynman−Vernon influence functional path integrals provide a numerically exact approach for

https://doi.org/10.1021/acs.jctc.6c00030
J. Chem. Theory Comput. 2026, 22, 3827−3838

simulating these systems interacting with potentially multiple baths.[31] For a separable initial condition $\rho(0) = \rho_{sys}(0)\, e^{-\beta \hat{H}_{bath}}/Z_{bath}$, the time-evolved reduced density matrix corresponding to the system can be written as[7,8]

$$\langle s_N^+|\rho_{sys}(N\Delta t)|s_N^-\rangle = \sum_{s_0^\pm}\sum_{s_1^\pm}\cdots\sum_{s_{N-1}^\pm}\langle s_N^\pm|\mathcal{E}_0(\Delta t)|s_{N-1}^\pm\rangle \times \langle s_{N-1}^\pm|\mathcal{E}_0(\Delta t)|s_{N-2}^\pm\rangle\cdots\langle s_1^\pm|\mathcal{E}_0(\Delta t)|s_0^\pm\rangle\langle s_0^+|\rho_{sys}(0)|s_0^-\rangle F[\{s_j^\pm\}] \tag{5}$$

where $\mathcal{E}_0(\Delta t) = e^{-i\hat{H}_{sys}\Delta t/\hbar} \otimes e^{i\hat{H}_{sys}\Delta t/\hbar}$ is the dynamical map corresponding to the bare system, $s_j^\pm$ is the state of the system at the jth time point and $F[\{s_j^\pm\}]$ is the Feynman-Vernon influence functional along the path $\{s_j^\pm\}$.[31] The influence functional F is dependent on the bath response function and consequently also on the spectral density as specified in eq 4. It accounts for the non-Markovian effects of the environment and can be calculated analytically for harmonic baths[7] or estimated using semiclassical or classical trajectories[35−37] for atomistic baths.

Additionally, to complete the description of the problem, often the system-bath couple (eq 1) is not isolated. It interacts with a larger universe and is, consequently, open to other processes (besides the rigorously described interactions with the bath). They may cause changes in the state of the system like spontaneous emission, pumping/loss of quantum particles, etc. While one can attempt to describe the atomistic details of such processes, this becomes an exceedingly challenging task. As long as one is interested solely in their impact on the preceding transport, such a careful parametrization of these processes may be unnecessary. One can choose to include these processes on an "empirical" level by incorporating a rough time-scale through Lindblad jump operators that interact with the system. Without loss of generality, one can presume that the Lindblad jump operators are constructed as a sum of elementary jump operators of the form:

$$L_n = T_n^{-1/2}\sum_j \tilde{L}_{nj} \tag{6}$$

$$\tilde{L}_{nj} = c_{nj}|f_{nj}\rangle\langle i_{nj}| \tag{7}$$

where T_n is the time-scale of action of the nth jump operator, c_{nj} is some coefficient and $|i_{nj}\rangle$ and $|f_{nj}\rangle$ are system states. (On a cautionary note, while this might be a fair zeroth order approximation to treat the "external interactions" through Lindblad jump operators, because we are primarily interested in the transport in the aggregate, one cannot, in general, treat the influence of vibrational and solvent degrees of freedom on the system using Lindblad operators. The Lindblad quantum master equation is an intrinsically Markovian equation of motion and is consequently unable to capture the non-Markovian and nonperturbative influence of the bath as shown in eq 5.)

In the presence of such external empirical processes, the equation of motion for the reduced density matrix of such a system-bath set is given by the Lindblad master equation:[32,33]

$$\dot{\rho}(t) = -\frac{i}{\hbar}[\hat{H}, \rho(t)] + \sum_n \left(L_n\rho(t)L_n^\dagger - \frac{1}{2}\{L_n^\dagger L_n, \rho(t)\}\right) \tag{8}$$

where $\rho(t)$ is a function of the system ($s^\pm$) and bath ($x^\pm$) degrees of freedom, that is,

$$\rho(t) = \sum_{s^\pm}\int\cdots\int dx^\pm|s^+, x^+\rangle\langle s^+, x^+|\rho(t)|s^-, x^-\rangle\langle s^-, x^-|$$

At this stage, it is useful to emphasize the triple-layered nature of the full universe that is involved in this description — we have the system layer, the bath comprising of the vibrational and solvent degrees of freedom, and the external universe which interacts with the system through the Lindblad jump operators. Naïvely solving eq 8 while propagating both the system and bath degrees of freedom in an exact manner is computationally infeasible because of the exponential scaling with respect to the dimension of the system-bath Hilbert space. Our recently developed PILD method[30] offers a convenient approach to extending QuAPI[7,8] to incorporate empirical Lindblad operators in addition to the thermal baths by replacing the bare system propagator, $\mathcal{E}_0(\Delta t)$, in eq 5 with the forward−backward system propagator in the presence of the Lindblad master equation. It, therefore, allows for the simulation of the RDM corresponding to the system, $\rho_{sys}(t) = \mathrm{Tr}_{bath}[\rho(t)]$, where $\rho(t)$ is the RDM corresponding to the system-bath portion satisfying eq 8 with $\rho(0) = \rho_{sys}(0)\, e^{-\beta \hat{H}_{bath}}/Z_{bath}$.

According to PILD,[30] if one assumes that the memory kernel induced by the vibrational and solvent bath is unperturbed by the phenomenological processes, the equation of motion can be expressed as a modified Nakajima-Zwanzig master equation:

$$\dot{\rho}_{sys}(t) = -\frac{i}{\hbar}[\hat{H}_{sys}, \rho_{sys}] + \int_0^{\tau_{mem}}\mathcal{K}(\tau)\rho_{sys}(t-\tau)d\tau + \sum_n\left(L_n\rho_{sys}(t)L_n^\dagger - \frac{1}{2}\{L_n^\dagger L_n, \rho_{sys}(t)\}\right) \tag{9}$$

where $\mathcal{K}(\tau)$ is the non-Markovian memory kernel and τ_{mem} is the memory length. This memory kernel can be obtained accurately from approximate[38,39] or numerically exact[40] simulations of the time evolution of $\rho_{sys}(t)$ in the absence of the Lindbladians. Alternatively, one can use the transfer tensor method[41] to link the dynamical map of the reduced system in the presence of the solvent environment, $\mathcal{E}(t)$ where $\rho_{sys}(t) = \mathcal{E}(t)\rho_{sys}(0)$, to transfer tensors, that are analogous to time-discretized versions of the memory kernel. One can now use any path integral method to simulate the dynamical map of the system-bath set in absence of the Lindbladians and extract from there the solvent memory kernel. (It is trivial to modify eq 5 to yield the dynamical maps by removing the sum over $s_0^\pm$ and removing the initial reduced density matrix factor.) On solving eq 9 with the desired Lindblad jump operators, one obtains the combined effect of the non-Markovian solvent environment and the Markovian empirical Lindblad processes.

In this paper we ask a slightly different question: beyond the population dynamics obtained from $\rho_{sys}(t)$, is it possible to inquire into the routes of transport that the system shows in the presence of both the bath and the external empirical process? Our state-to-state analysis framework[21] provides a way to answer this question. Here we try to apply the same logic to the system-bath problem subject to empirical pumps and drains.

We start by analyzing the rate of change of the population of a particular system state. Using eq 8, the time derivative of the population of system state $|l\rangle$ can be written as

https://doi.org/10.1021/acs.jctc.6c00030
J. Chem. Theory Comput. 2026, 22, 3827−3838

$$\begin{aligned}\dot{P}_l(t) &= \langle l|\dot{\rho}_{\text{sys}}(t)|l\rangle \\ &= \langle l|\text{Tr}_{\text{bath}}[\dot{\rho}(t)]|l\rangle \\ &= \dot{P}_l^H(t) + \dot{P}_l^L(t)\end{aligned} \tag{10}$$

where we have split the expression between terms arising out of the commutator with the Hamiltonian, $\dot{P}_l^H(t)$, and ones arising from the Lindbladian terms, $\dot{P}_l^L(t)$. Therefore,

$$\begin{aligned}\dot{P}_l^H(t) &= -\frac{i}{\hbar}\langle l|\text{Tr}_{\text{bath}}([\hat{H}, \rho(t)])|l\rangle \\ &= -\frac{i}{\hbar}\sum_r (\langle l|\hat{H}_{\text{sys}}|r\rangle\langle r|\rho_{\text{sys}}(t)|l\rangle - \langle l|\rho_{\text{sys}}(t)|r\rangle\langle r|\hat{H}_{\text{sys}}|l\rangle)\end{aligned} \tag{11}$$

$$\begin{aligned}\dot{P}_l^L(t) &= \sum_n \langle l|\left(L_n\rho_{\text{sys}}(t)L_n^\dagger - \frac{1}{2}\{L_n^\dagger L_n, \rho_{\text{sys}}(t)\}\right)|l\rangle \\ &= \sum_n T_n^{-1}\sum_{j,k} c_{nj}c_{nk}^*\Big(\langle i_{nj}|\rho_{\text{sys}}(t)|i_{nk}\rangle\delta_{l,f_{nj}}\delta_{l,f_{nk}} \\ &\quad - \frac{1}{2}\delta_{f_{nj},f_{nk}}(\delta_{l,i_{nj}}\langle i_{nk}|\rho_{\text{sys}}(t)|l\rangle + \delta_{l,i_{nk}}\langle l|\rho_{\text{sys}}(t)|i_{nj}\rangle)\Big)\end{aligned} \tag{12}$$

The simplification done in eq 11 is only possible in the case of diagonal system-bath coupling operator, $\hat{H}_{\text{sys-bath}}$. This is consistent with the Frenkel-Holstein model of exciton dynamics or the system-bath decompositions conventionally used to describe charge transfer processes. (See Appendix B for an alternative derivation of eq 11 which highlights why it consists of only $\hat{H}_{\text{sys}}$ and $\rho_{\text{sys}}(t)$ terms.) Equation 12 uses the fact that the Lindblad jump operators considered act only on the Hilbert space of the system. Thus, in representing both the Hamiltonian and the Lindbladian contributions to the rate of change in terms of $\rho_{\text{sys}}(t)$, we have been able to relax our requirement of knowing the dynamics corresponding to the system-bath couple. Even though the system RDM $\rho_{\text{sys}}(t)$ satisfies the non-Markovian equation 9, the population derivative does not depend upon the memory kernel at all. Now, $\dot{P}_l(t)$ in eq 10 can be computed from $\rho_{\text{sys}}(t)$, $\hat{H}_{\text{sys}}$, and the empirical Lindblad jump operators. Therefore, methods like PILD that simulate $\rho_{\text{sys}}(t)$ directly can be used to obtain the relevant dynamics.

Now to complete the state-to-state analysis, we need to be able to partition the rate of change of population of state $|l\rangle$ in terms of other states $|r\rangle$:

$$\dot{P}_l(t) = \sum_r \dot{P}_{l\leftarrow r}(t) \tag{13}$$

where $\dot{P}_{l\leftarrow r}(t)$ is the instantaneous rate of change of the population of the lth site due to the rth site. This is achieved trivially for $\dot{P}_l^H(t)$, which already has this structure in eq 11. However, notice that for $\dot{P}_l^L(t)$ in eq 12, this partitioning is not possible. There are summations over two states, $|i_{nk}\rangle$ and $|i_{nj}\rangle$ for each Lindbladian L_n which may contribute to the flux of system state $|l\rangle$. How does one choose a unique system state $|r\rangle$ and decompose the population flux as in eq 13?

The ambiguity and complexity stemming from the multiple states $|i_{nk}\rangle$, $|i_{nj}\rangle$, and the extra summation over different Lindbladians can all be traced to our definitions of the jump operators as an unconstrained sum of elementary Lindbladians. Such a description is more general than required for dealing with simple empirical pumping and draining processes. (Remember that the thermal solvent is accounted for by some numerically exact non-Markovian quantum dynamics method, leaving only the simplest of empirical processes to be relegated to the Markovian Lindbladian approximations.) To understand the action of multiple such processes and the practical restrictions that one might impose on them, consider an exciton transport system with multiple extraction points. The key idea we want to consider is the spatial locality of the empirical processes. If we drain or pump the jth site through a process, a different site k would typically not be affected. This means that the initial state that a particular process acts on uniquely defines the final state. Suppose the process under consideration is draining a site. In this case, it uniquely takes the first excited state of this molecule to the ground state. On the other hand, if this was a pumping process, it will uniquely take this molecule from the ground to the excited state. Of course, the full many-body operator would be defined as the direct product of this one-body operator with identities on all the other sites. This is what we want to encode in our empirical Lindbladians.

Motivated by the site- and state- specific nature of pumping and draining processes, we put a single, probably weaker, physical restriction on them: if two elementary jump operators $\tilde{L}_{nj}$ and $\tilde{L}_{nj'}$ are part of a single jump operator L_n (signifying the nth process), then they cannot have the same end-point. Mathematically, if $j \neq k$, then for all n, $|f_{nj}\rangle \neq |f_{nk}\rangle$. In other words, a single process L_n should not map two different initial states to the same final state. Processes mapping different initial states (whether on the same or different sites) to the same final state would, in a plurality of cases, be better represented by two different Lindbladians L_n and $L_{n'}$ owing to different external environment modes accounting for them. This serves as the minimal criterion that can account for most such pumping/draining processes, and also gets rid of the double summation over j and k in eq 12. Thus, upon simplification, eq 10 gives

$$\begin{aligned}\dot{P}_l(t) &= -\frac{2}{\hbar}\sum_r \langle l|\hat{H}_{\text{sys}}|r\rangle\text{Im}\langle l|\rho_{\text{sys}}(t)|r\rangle \\ &\quad + \sum_n T_n^{-1}\sum_j |c_{nj}|^2\langle i_{nj}|\rho_{\text{sys}}(t)|i_{nj}\rangle(\delta_{l,f_{nj}} - \delta_{l,i_{nj}})\end{aligned} \tag{14}$$

In the light of eq 14, let us now rewrite the Lindbladian contribution to the population flux:

$$\dot{P}_l^L(t) = \sum_n T_n^{-1}\sum_j |c_{nj}|^2\langle i_{nj}|\rho_{\text{sys}}(t)|i_{nj}\rangle(\delta_{l,f_{nj}} - \delta_{l,i_{nj}}) \tag{15}$$

To understand how to decompose it in a state-specific manner, consider the effect of a single elementary Lindbladian $T^{-1/2}|f\rangle\langle i|$, which causes population to flow from the ith state to the fth state. Below are the rates of change of these two states caused only by the Lindbladian terms. (The Hamiltonian part has been suppressed.)

$$\dot{P}_f^L(t) = T^{-1}\langle i|\rho_{\text{sys}}(t)|i\rangle \tag{16}$$

$$\dot{P}_i^L(t) = -T^{-1}\langle i|\rho_{\text{sys}}(t)|i\rangle \tag{17}$$

The origins of eqs 16 and 17 are in the first and second Lindbladian terms of eq 15 respectively. As expected, the rate of change of the population of the ith state is negative, and that of the fth state is positive reflecting the direction of the population flow. Now to assign the "source" of these changes, notice that the Lindbladian causes population to flow from $|i\rangle$

https://doi.org/10.1021/acs.jctc.6c00030
J. Chem. Theory Comput. 2026, 22, 3827−3838

to $|f\rangle$). Consequently, $\dot{P}_i^L(t)$ must be caused by the fth state, and $\dot{P}_f^L(t)$ must have as its source the ith site. Thus, the source-resolved population flux equation would be given by

$$\dot{P}_{l\leftarrow r}(t) = -\frac{2}{\hbar}\langle l|\widehat{H}_{\text{sys}}|r\rangle \text{Im}\langle l|\rho_{\text{sys}}(t)|r\rangle + \sum_n T_n^{-1}\sum_j |c_{nj}|^2\langle i_{nj}|\rho_{\text{sys}}(t)|i_{nj}\rangle(\delta_{l,f_{nj}}\delta_{r,i_{nj}} - \delta_{l,i_{nj}}\delta_{r,f_{nj}}) \tag{18}$$

The final step is where the expressions are integrated to obtain the direct and unmediated transport from a state $|r\rangle$ to a state $|l\rangle$.

$$P_{l\leftarrow r}(t) = -\frac{2}{\hbar}\langle l|\widehat{H}_{\text{sys}}|r\rangle \int_0^t \text{d}t' \text{Im}\langle l|\rho_{\text{sys}}(t')|r\rangle + \sum_n T_n^{-1}\sum_j \int_0^t \text{d}t'\langle i_{nj}|\rho_{\text{sys}}(t')|i_{nj}\rangle|c_{nj}|^2\delta_{l,f_{nj}}\delta_{r,i_{nj}} - \sum_n T_n^{-1}\sum_j \int_0^t \text{d}t'\langle i_{nj}|\rho_{\text{sys}}(t')|i_{nj}\rangle|c_{nj}|^2\delta_{l,i_{nj}}\delta_{r,f_{nj}} \tag{19}$$

This is the final form of the Lindblad state-to-state formalism. The first term of eq 19 is exactly the same as the traditional state-to-state transport.[21] It accounts for the rate at which the population is transferred from $|r\rangle$ to $|l\rangle$ via the Hamiltonian. This we will call the Hamiltonian transport or the Hamiltonian flow. Additional transport happens through the jump operators, which we will call the Lindbladian transport or flow.

Next consider the two Lindbladian transport terms in eq 19 separately. They show the total change in the population of the lth state due to various jump operators, if the ending state is $|l\rangle$ and the starting state is $|r\rangle$. Specifically, the first Lindbladian term talks about the total increase in the population of the lth site because of the rth site through all the Lindblad mechanisms while the second term talks about the total decrease in the population of the lth site because of the total Lindbladian flow from the lth to the rth site. These two terms together constitute the net Lindbladian transport.

Equation 19 can be shown to be consistent with the principle of detailed balance, $P_{l\leftarrow r}(t) = -P_{r\leftarrow l}(t)$. Also, $P_{l\leftarrow l}(t) = 0$ showing that no self-transfer can happen. Moreover, since eq 19 is expressed in terms of $\hat{H}_{\text{sys}}$ and $\rho_{\text{sys}}(t)$, it remains valid even for the case when no explicit bath is there. For the purposes of this paper, we are going to concentrate on pumping and draining processes acting on a system-bath couple, and numerically explore the consequences of eq 19.

3. NUMERICAL RESULTS

We will demonstrate the Lindblad state-to-state analysis method through a series of examples pertaining to polaritonic and excitonic dynamics. First, in Section 3.1, we will demonstrate the consistency of the current method with the recently developed non-Hermitian state-to-state[29] analysis method for the set of mutually applicable problems. Then we move on to examples where the non-Hermitian state-to-state analysis is not applicable—we demonstrate the Lindblad state-to-state method using the case of an excitonic dimer being pumped (Section 3.2), and then simultaneously pumped and drained from different sites (Section 3.3). We use our PILD method[30,42] implemented through the `QuantumDynamics.jl` package[43] to obtain $\rho_{\text{sys}}(t)$ for all simulations presented herein. The time-evolved matrix product operators (TEMPO)[11] implementation of QuAPI is used to simulate the dynamical maps required for PILD.

3.1. Comparison with non-Hermitian State-to-State

Both the current Lindblad state-to-state approach and the recently published non-Hermitian state-to-state approach[29] seem to enable exploration of routes of transport and transport efficiencies for open quantum systems with empirically described loss processes. In the previous work, those processes were described by non-Hermiticities, whereas here, they are described by the Lindblad jump operators. While the non-Hermitian method may be able to get away with a smaller system dimensionality in certain cases, the Lindblad approach is significantly more general as we shall demonstrate through later numerical examples. (This difference of the Lindblad approach over the non-Hermitian description is also discussed in Appendix A.) The common pool of problems that both the approaches can deal with are cases where the only empirical processes impacting the system are one or more loss (drain) sites. We, therefore, use such a case to validate our Lindblad state-to-state method.

It should be noted at the outset that both the methods have different empirical ways of incorporating the losses. There cannot be a guarantee of getting identical results. The check, therefore, is one of consistency of conclusions obtained from either methods. In the limit of extremely weak empirical processes both methods should become identical. In our numerical exploration, we show that surprisingly all the observables turn out to be the same between the non-Hermitian and the Lindbladian treatments.

Consider a nearest-neighbor polaritonic trimer where an excitonic trimer is coupled to a Fabry-Pérot cavity mode described by the Tavis-Cummings Hamiltonian:[44]

$$\widehat{H}_{\text{sys}} = \epsilon_0|0\rangle\langle 0| + \sum_j \epsilon_j|j\rangle\langle j| + \sum_{j<k} h_{jk}(|j\rangle\langle k| + |k\rangle\langle j|) + \hbar\omega_c|c\rangle\langle c| + \sum_j \Omega(|j\rangle\langle c| + |c\rangle\langle j|) \tag{20}$$

where $|0\rangle$ is the ground state of the system, $|j\rangle$ represents the state where the excitation is on the jth monomer and $|c\rangle$ is the cavity mode. The Tavis−Cummings Hamiltonian[44] models the impact of a single cavity mode under the dipolar (or long wavelength) approximation. More accurate simulations of polaritonic transport would require going beyond this model.[45−48] The parameters are taken to be same as one of the examples from ref 29, which we summarize here for convenience. The energy of the ground state ϵ_0 is taken to be 0 cm^{-1}. All the monomers are assumed to be identical with the same excitation energies. Therefore, ϵ_j is independent of the site number j. Because, we are interested in the dynamics starting from a first-excitation subspace state, we can set $\epsilon_j = 0$ cm^{-1} for all j. The nearest-neighbor intermonomer coupling is taken as $h_{j,k} = -h = -181.5\ \text{cm}^{-1}\delta_{k,j+1}$. The exciton is harvested from the third monomer or $|3\rangle$ with a time-scale of $T_3 = 300$ fs. The cavity is taken to be resonant with the molecular Franck−Condon excitation energy, that is, $\hbar\omega_c = \epsilon_j = 0$ cm^{-1} with a coupling strength of $\Omega = 181.5$ cm^{-1}. All Fabry−Pérot cavities, typically, have a certain time-scale with which they lose the photon. Such a loss diverts a part of the excitonic transport, as the photon is never truly harvested. Following the example in ref 29, we take the time-scale of loss from cavity to be $T_c = 600$

https://doi.org/10.1021/acs.jctc.6c00030
J. Chem. Theory Comput. 2026, 22, 3827−3838

fs, and model the molecular nuclear environment for each monomer using the Ohmic spectral density:

$$J(\omega) = 2\pi\hbar\xi\omega\exp(-\omega/\omega_{\text{cutoff}}) \tag{21}$$

where the Kondo parameter $\xi = 0.121$ and $\omega_{\text{cutoff}} = 900\ \text{cm}^{-1}$ corresponding to a reorganization energy $\lambda_0 = 217.8\ \text{cm}^{-1}$. The cavity mode is of course not associated with any bath. All the simulations are done at a temperature of 300 K. In presence of these vibrational baths, the model is often referred to as the Holstein−Tavis−Cummings model.[44]

The losses on the third monomer and the cavity are incorporated in different ways for the two methods. For the non-Hermitian system, ϵ_3 and ω_c are made complex with $\text{Im}(\epsilon_3) = -\pi\hbar/T_3$ and $\text{Im}(\omega_c) = -\pi/T_c$.[29] The Lindbladian description is more elaborate. The two losses are accounted for by two different jump operators

$$L_3 = T_3^{-1/2}|0\rangle\langle 3| \tag{22}$$

$$L_c = T_c^{-1/2}|0\rangle\langle c| \tag{23}$$

Notice that unlike the non-Hermitian case where the target site of the losses is undetermined, for the Lindblad method we explicitly state that both the jump operators bring the system down into the same state $|0\rangle$. (Note that $|0\rangle$ is not even included in the non-Hermitian calculations.) We first show the dynamics obtained from both the methods in Figure 1, which

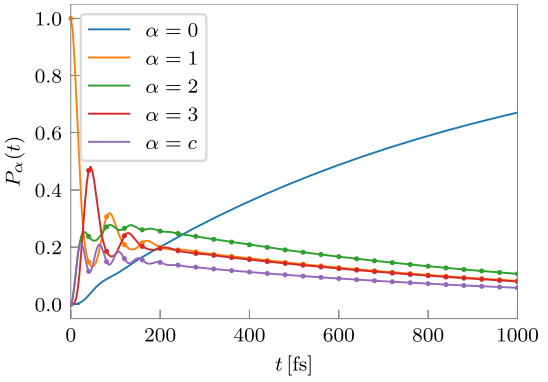

Figure 1. Population, $P_\alpha(t)$, of different states $|\alpha\rangle$ in a polaritonic trimer with an initial excitation $\rho_{\text{sys}}(0) = |1\rangle\langle 1|$. (Markers: non-Hermitian state-to-state results;[29] lines: Lindblad state-to-state results).

match exactly. A time-step of $\Delta t = 4$ fs and a non-Markovian memory length of $\tau_{\text{mem}} = 200$ fs (amounting to 50 time-steps) were used for the converged dynamics in both cases. However, the increase of the ground state population due to the losses is a feature that is captured only by the PILD method.[30]

Next, we compare the state-to-state analysis obtained from both the methods in Figure 2, excluding the loss terms. We have previously analyzed the physics of this problem in depth[29] and avoid going into the details. Notice that the results obtained from the Lindblad state-to-state method matches those obtained from our non-Hermitian state-to-state method.

There is, however, an intrinsic difference in the interpretation of the loss terms between the non-Hermitian state-to-state approach and the current approach. As discussed, the non-Hermitian approach does not necessitate the inclusion of the ground state $|0\rangle$; loss, $\mathcal{L}_j(t)$, from a site j is given by $|P_{j\leftarrow j}(t)|$. However, for the Lindblad state-to-state picture (eq 19), it can

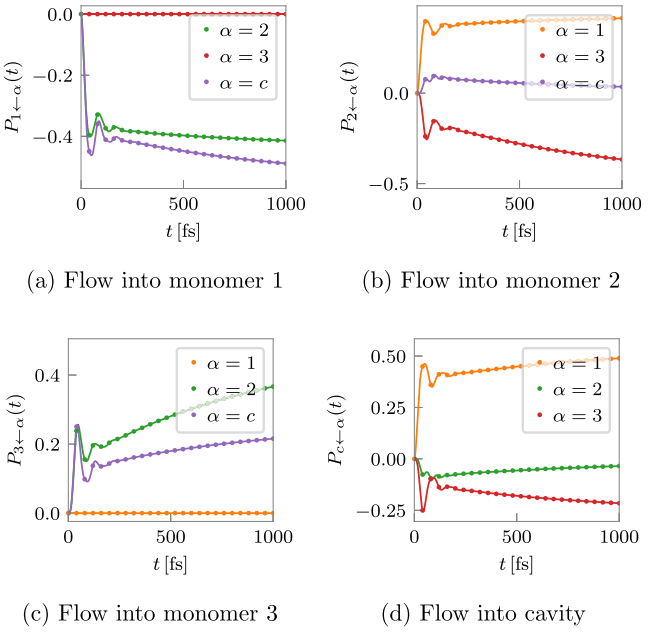

Figure 2. State-to-state analysis of excitation flows into different sites, (a−d), of the lossy polaritonic trimer. (Lines: Lindblad state-to-state result; markers: non-Hermitian state-to-state results;[29] orange: $P_{*\leftarrow 1}(t)$, green: $P_{*\leftarrow 2}(t)$, red: $P_{*\leftarrow 3}(t)$, and purple: $P_{*\leftarrow c}(t)$. Terms of the type $P_{\alpha\leftarrow\alpha}(t)$ are not depicted here).

be trivially shown that $P_{j\leftarrow j}(t) = 0$. Loss, here, is seen as a Lindbladian transport of the system from the jth site to the ground state, $\mathcal{L}_j(t) = P_{0\leftarrow j}(t)$. In Figure 3, we show the loss

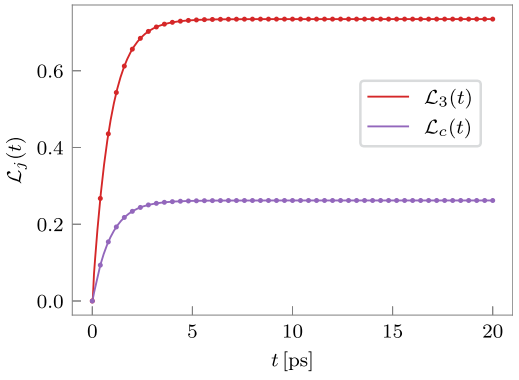

Figure 3. Site-specific excitation loss, $\mathcal{L}_j(t)$, from the polaritonic trimer. Lines: Lindblad state-to-state, markers: non-Hermitian method.[29]

from $|j\rangle$ for $j = 3, c$ using both the methods, which are once again identical. Additionally, as expected, there is no loss from sites 1 and 2 into the ground state (not included therefore in Figure 3).

This example demonstrates the equivalence of the Lindblad state-to-state method and the non-Hermitian state-to-state method for the subset of problems where both methods are applicable.

3.2. Pumped Excitonic Dimer

Next we move onto the first case where the current method is uniquely applicable. Imagine an excitonic dimer that is initially in the ground state. The left monomer (monomer 1) is pumped incoherently with a particular time-scale, T_{pump}. We

https://doi.org/10.1021/acs.jctc.6c00030
J. Chem. Theory Comput. 2026, 22, 3827−3838

want to understand the flow of excitation into this system. Unlike in our previous example, this system can no longer be described using the first excitation subspace. That is because the number of excitation keeps rising until we have two excitations (or N excitations for an N-mer in general).

The full space Hamiltonian for an N-mer with identical monomers and only nearest-neighbor couplings, $h_{j,k} = -h = -181.5\ \mathrm{cm}^{-1}\delta_{k,j+1}$, can be written in terms of the localized diabatic basis formed by the direct products of $|g_j\rangle$ and $|e_j\rangle$ denoting the molecular ground and excited states, respectively, on the jth monomer as

$$\hat{H}_{\mathrm{sys}} = \epsilon \sum_{j=1}^{N} |e_j\rangle\langle e_j| - h \sum_{j=1}^{N-1} (|e_j g_{j+1}\rangle\langle g_j e_{j+1}| + |g_j e_{j+1}\rangle\langle e_j g_{j+1}|) \tag{24}$$

where $\epsilon = 1000\ \mathrm{cm}^{-1}$ is the monomeric excitation energy. Each of these monomers are once again coupled to the same Ohmic vibrational bath as before (eq 21). For such an N-mer, any pump on a site j can be written as $L_j^{\mathrm{pump}} = T_{\mathrm{pump}}^{-1/2}|e_j\rangle\langle g_j|$ while a drain on site j can be written as $L_j^{\mathrm{drain}} = T_{\mathrm{drain}}^{-1/2}|g_j\rangle\langle e_j|$.

For the excitonic dimer defined using eq 24 for $N = 2$, the excitation pump at the left monomer can be written in an expanded fashion as $L_1^{\mathrm{pump}} = T_{\mathrm{pump}}^{-1/2}(|eg\rangle\langle gg| + |ee\rangle\langle ge|)$, where $T_{\mathrm{pump}} = 300$ fs. The two terms in the Lindbladian correspond to a pumping into the first excitation subspace from the ground state, and from the first excitation subspace to the doubly excited state, respectively.

The dynamics from an initially unexcited excitonic dimer, $\rho_{\mathrm{sys}}(0) = |gg\rangle\langle gg|$, is shown in Figure 4. Convergence was

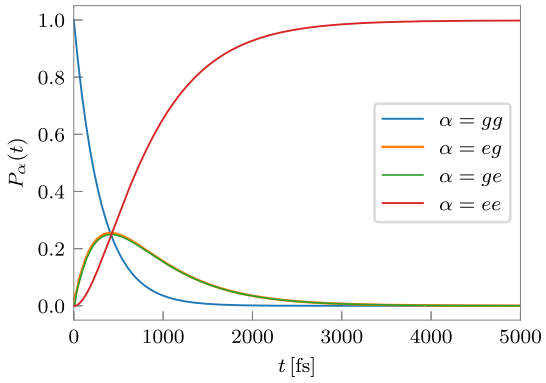

Figure 4. Population, $P_\alpha(t)$, of different states $|\alpha\rangle$ in the excitonic dimer initially in the ground state, $\rho_{\mathrm{sys}}(0) = |gg\rangle\langle gg|$, with excitation being pumped into monomer 1 with a time-constant of $T_{\mathrm{pump}} = 300$ fs.

reached at a time-step of $\Delta t = 4$ fs and a memory time of $\tau_{\mathrm{mem}} = 400$ fs. The system starts from $|gg\rangle$, but soon gains excitation. Because there are no excitonic drains, eventually all the population moves into the doubly excited state $|ee\rangle$. The population of $|eg\rangle$ increases slightly before $|ge\rangle$ because it is the state that is getting pumped. The state $|ge\rangle$ gains population through a Hamiltonian transfer from the $|eg\rangle$ state because of the nearest-neighbor coupling. The effective time scale of accumulation of excitation in the dimer τ_{total} comes out to be 602 fs assuming a model fit

$$\mathcal{E}_{\mathrm{total}}(t) = \mathcal{E}_{\mathrm{total}}^{\infty}(1 - \exp(-t/\tau_{\mathrm{total}}))$$

where

$$\mathcal{E}_{\mathrm{total}}(t) = \sum_{\alpha} \mathcal{E}_\alpha(t) = \sum_{\alpha} \mathrm{Tr}_{\mathrm{sys}}[\rho_{\mathrm{sys}}(t)|e_\alpha\rangle\langle e_\alpha|]$$

is the total excitation in the system.

The state-to-state analysis in the diabatic basis for this pumped dimer is shown in Figure 5. Consistent with the

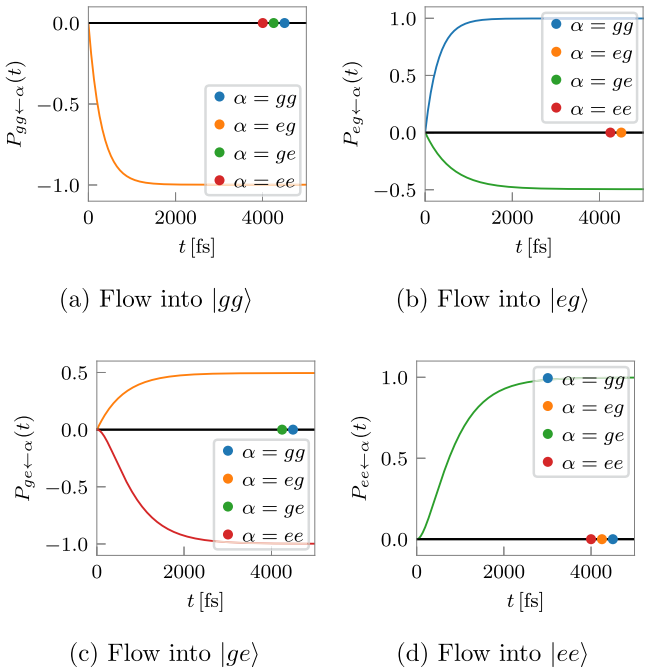

Figure 5. State-to-state analysis of excitation flows into the diabatic states, (a−d), of the excitonic dimer when pumped with $T_{\mathrm{pump}} = 300$ fs. (Blue: $P_{*\leftarrow gg}(t)$, orange: $P_{*\leftarrow eg}(t)$, green: $P_{*\leftarrow ge}(t)$, and red: $P_{*\leftarrow ee}(t)$. Black indicates multiple overlapping curves with legends marked as discs of corresponding colors.).

Lindblad jump operators, the pumping procedure takes the system from $|gg\rangle$ to $|eg\rangle$. The $|ge\rangle$ state only receives population from the $|eg\rangle$ state. There is also only a single route of transport into $|ee\rangle$, which is from $|ge\rangle$ and Lindbladian in origin.

Finally, in these kinds of problems, it is also interesting to think about the excitation flows not between the diabatic states, but in terms of the molecules. We would, for instance, like to ask what is the net flow of exciton into the first monomer. The diabatic state-to-state analysis discussed above gives a perfect starting point for answering these questions. The flow of excitation into the first monomer, $\mathcal{F}_1^+(t)$, through the pumping mechanism can be trivially shown to be $P_{eg\leftarrow gg}(t) + P_{ee\leftarrow ge}(t)$. (Assuming a model fit $\mathcal{F}_1^+(t) = \mathcal{F}_1^\infty(1 - \exp(-t/\tau_1))$ gives an effective pumping rate τ_1 into monomer 1 to be 602 fs which is same as that for the accumulation of excitation in the dimer, $\mathcal{E}_{\mathrm{total}}(t)$.) In a similar manner, the flow of excitation from the first to the second monomer, $\mathcal{F}_{2\leftarrow 1}(t)$, is just $P_{ge\leftarrow eg}(t)$. These flows are shown in Figure 6. The flow into the first monomer is positive as is the flow from monomer 1 to 2.

3.3. Simultaneous Pumping and Draining

As a last class of problems, let us move on to a system being simultaneously pumped and drained of excitation from two different sites. Consider the same excitonic dimer prepared in

https://doi.org/10.1021/acs.jctc.6c00030
J. Chem. Theory Comput. 2026, 22, 3827−3838

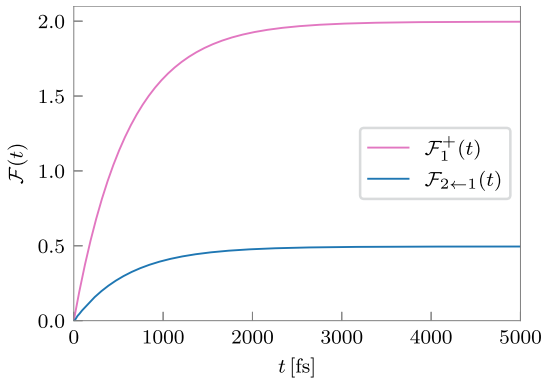

Figure 6. Total excitation flows into the first monomer, $\mathcal{F}_1^+(t)$, and from monomer 1 to 2, $\mathcal{F}_{2\leftarrow1}(t)$, of the excitonic dimer being pumped from monomer 1 with corresponding time scale T_{pump} = 300 fs.

ground state as discussed in Section 3.2 which, in addition to being pumped from monomer 1, is now also being drained from monomer 2 which are accounted for by the Lindblad jump operators:

$$L_1^{\text{pump}} = T_{\text{pump}}^{-1/2}(|eg\rangle\langle gg| + |ee\rangle\langle ge|) \tag{25}$$

$$L_2^{\text{drain}} = T_{\text{drain}}^{-1/2}(|gg\rangle\langle ge| + |eg\rangle\langle ee|) \tag{26}$$

We start by exploring the time-evolution of the excitation population, $\mathcal{E}_\alpha(t) = \text{Tr}_{\text{sys}}[\rho_{\text{sys}}(t)|e_\alpha\rangle\langle e_\alpha|]$, on the monomers α in Figure 7 for three different combinations of pumping and

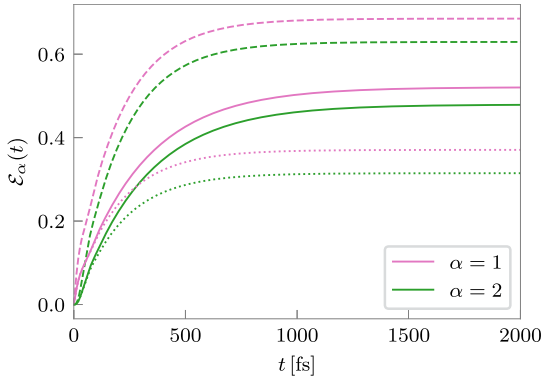

Figure 7. Total excitation $\mathcal{E}_\alpha(t)$ accumulated on the monomer α in the excitonic dimer being pumped and drained simultaneously from monomers 1 and 2, respectively, with corresponding time scales (T_{pump}, T_{drain}) of (150 fs, 300 fs) (dashed), (300 fs, 300 fs) (solid), and (300 fs, 150 fs) (dotted).

draining time-scales. Trivially, when the pumping rate is faster than draining rate, then the rise of the excitation population in the system is the largest. Notice that for each of these combinations, a steady-state is reached in the system.

Before analyzing the dynamics further using the state-to-state method, let us try to explore the steady state a bit more. We plot the total excitation ($\sum_\alpha \mathcal{E}_\alpha(t)$) at long-times (after the steady-state has set in) in Figure 8 as a function of the pumping and the draining time-scales. Along the diagonal characterized by $T_{\text{pump}} = T_{\text{drain}}$, one notices that the system has exactly a single excitation at steady-state. When $T_{\text{pump}} > T_{\text{drain}}$, the excitation population is less than one, and it is greater than one otherwise. Our preliminary explorations indicate that so

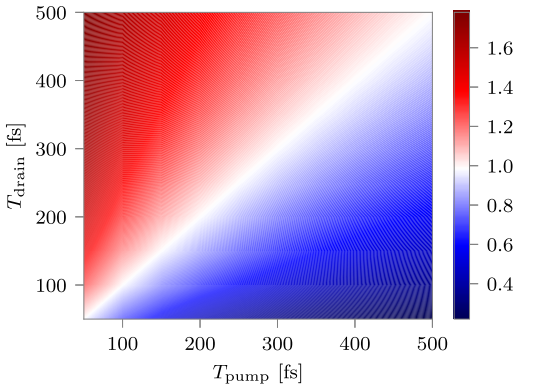

Figure 8. Total steady-state excitation accumulated in the excitonic dimer for different pumping and decay time-scales.

long as the system is homogeneous (that is the monomers are identical) these values are independent of the type of vibrational bath and only dependent on the system description.

For making our state-to-state discussions concrete, let us pick the case of $T_{\text{pump}} = T_{\text{drain}}$ = 300 fs. For this case, the converged dynamics was recovered at Δt = 2 fs and a memory time of τ_{mem} = 60 fs. In Figure 9, we show the state-to-state

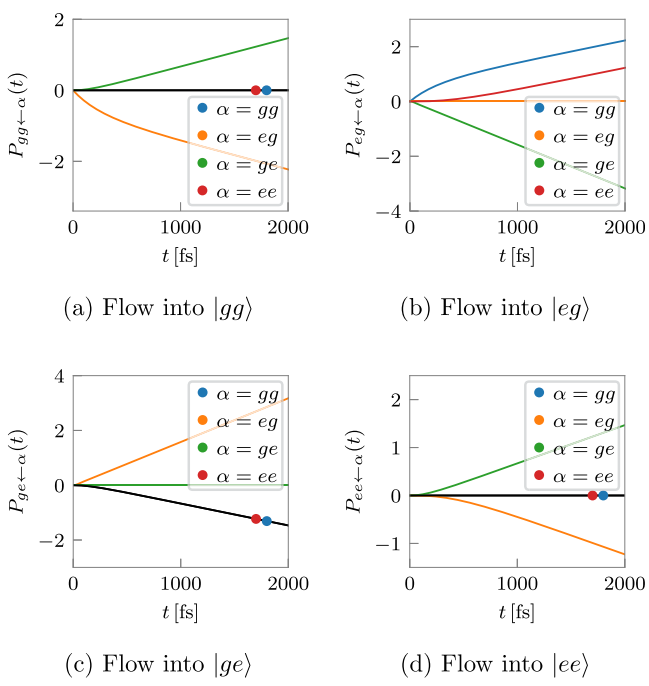

Figure 9. State-to-state analysis of excitation flows into different diabatic states, (a–d), of the excitonic dimer when simultaneously pumped and drained with $T_{\text{pump}} = T_{\text{drain}}$ = 300 fs. (Blue: $P_{*\leftarrow gg}(t)$, orange: $P_{*\leftarrow eg}(t)$, green: $P_{*\leftarrow ge}(t)$, and red: $P_{*\leftarrow ee}(t)$. Black indicates multiple overlapping curves with legends marked as discs of corresponding colors.)

transfers in the diabatic basis. All the transfers to and from $|gg\rangle$ or $|ee\rangle$ are Lindbladian in origin, and the Hamiltonian transports occur between the $|eg\rangle$ and $|ge\rangle$ states. The interpretation is similar to the pure pumping case and therefore, we skip it. One feature that is different from the previous case and consequently, deserves mentioning is the existence of certain transport curves that asymptotically become straight lines, but with nonzero gradients (e.g., the

https://doi.org/10.1021/acs.jctc.6c00030
J. Chem. Theory Comput. 2026, 22, 3827−3838

Lindbladian transport into and from $|gg\rangle$). This means that there is a continuous transport either into or from that state. This is because the steady-states reached in these systems are dynamic, and a result of balancing of the pumping and draining processes, both of which individually proceed in their own ways.

At this stage, we switch to the state-to-state analysis defined in terms of the monomeric excitation flows. Given that we are interested in spatial transport of excitation across monomers, this is the more physically relevant basis. While the diabatic state-to-state transfers (Figure 9) are directly measured, as mentioned previously (in Section 3.2), the flow between the monomers can easily be reconstructed from them. This is presented in Figure 10. For our dimeric system, there are three

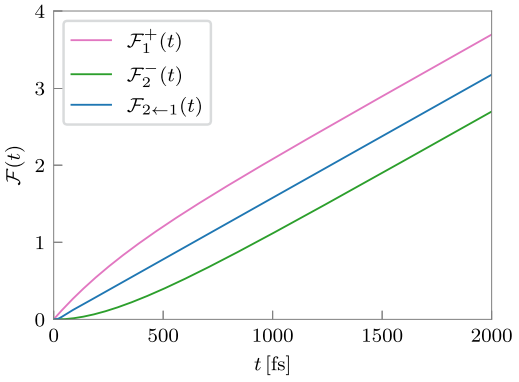

Figure 10. Total excitation flows into a monomer, $\mathcal{F}_\alpha^+(t)$, out of a monomer, $\mathcal{F}_\alpha^-(t)$, and between two monomers, $\mathcal{F}_{\alpha\leftarrow\beta}(t)$, of the excitonic dimer being pumped and drained simultaneously from monomers 1 and 2, respectively, with corresponding time scales $T_{\text{pump}} = T_{\text{drain}} = 300$ fs.

processes of interest—(a) the Lindbladian pumping of monomer 1 ($\mathcal{F}_1^+(t)$), (b) the Hamiltonian transport between monomers 1 and 2 ($\mathcal{F}_{2\leftarrow1}(t)$), and (c) the Lindbladian draining of monomer 2 ($\mathcal{F}_2^-(t)$). The total excitation content in the system at time t is $\mathcal{F}_1^+(t) - \mathcal{F}_2^-(t)$. The buildup of excitation in the system happens because of the time that it takes for the excitation to go from the pumping site to the draining site. The lines, $\mathcal{F}^\pm(t)$, becoming parallel is a signature of the steady-state setting in. Additionally, notice that because of the simultaneous pumping and draining, there is a net current of excitonic extraction from the second site. This is a feature that cannot be there for aggregates with only draining sites.

As a final example, we study two excitonic trimers (one defined as a nearest neighbor system with eq 24 for $N = 3$ and another defined with a 1−3 interaction of half the strength) with pumping and draining on the terminal sites (monomers 1 and 3, respectively). The flows in the monomeric picture are presented in Figure 11. A similar pattern emerges, except the steady-state excitation content of the excitonic trimer $\lim_{t\to\infty} \mathcal{F}_1^+(t) - \mathcal{F}_3^-(t)$ is 1.5 which is larger than 1.0 for the dimer. This value is irrespective of whether the intermonomer coupling is nearest neighbor or not. In case of the nearest neighbor trimer, we also notice that the only nonzero unmediated transports are between consecutive monomers. There is no direct flow between monomer 1 and monomer 3. However, in case of the non-nearest-neighbor

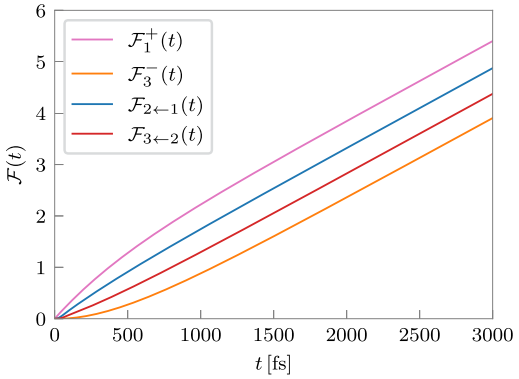

(a) Nearest-neighbor trimer

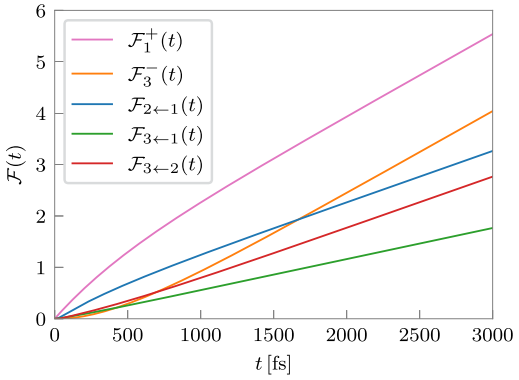

(b) Non-nearest-neighbor trimer

Figure 11. Total excitation flows into a monomer, $\mathcal{F}_\alpha^+(t)$, out of a monomer, $\mathcal{F}_\alpha^-(t)$, and between two monomers, $\mathcal{F}_{\alpha\leftarrow\beta}(t)$, of (a) the nearest-neighbor excitonic trimer and (b) the non-nearest neighbor excitonic trimer, being pumped and drained simultaneously from monomers 1 and 3, respectively, with corresponding time scales $T_{\text{pump}} = T_{\text{drain}} = 300$ fs.

trimer, because of the added coupling we begin to see a steady direct transfer between monomers 1 and 3. The rate of the nearest neighbor transport ($1 \leftarrow 2$ and $2 \leftarrow 3$) is around 1 ps^{-1}, whereas that of the $1 \leftarrow 3$ transport is 0.6 ps^{-1}.

In Figure 12 we show the extraction dynamics of the exciton from the dimer and nearest-neighbor trimer. Notice that if one defines the excitonic current as $I_{\text{exc}}(t) = \lim_{t\to\infty} \frac{d\mathcal{F}_{\text{drain}}(t)}{dt}$, then

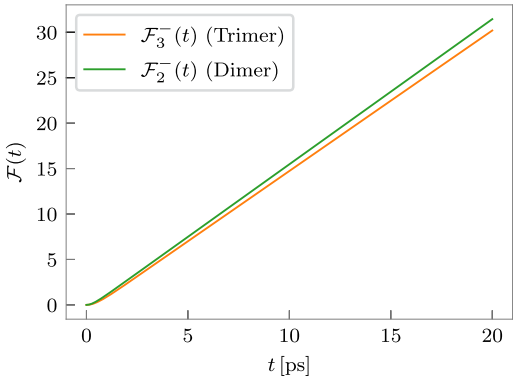

Figure 12. Excitation extraction as a function of time for the excitonic dimer and trimer with $T_{\text{pump}} = T_{\text{drain}} = 300$ fs.

https://doi.org/10.1021/acs.jctc.6c00030
J. Chem. Theory Comput. 2026, 22, 3827−3838

it is clear that the dimer provides a "higher" current (I_{exc}^{dimer} = 1.597 ps^{-1}) than the trimer (I_{exc}^{trimer} = 1.542 ps^{-1}) even though both are made of the same identical monomeric units. Coincidentally, introducing 1−3 coupling of half the strength of the nearest neighbor coupling increases the excitonic current to close to the value of the dimer. This size dependence and the other factors affecting the excitonic current would be further explored in a future work.

4. CONCLUSIONS

The state-to-state method[21,22] based on analysis of fluxes[2,49,50] has proven to be quite capable of elucidating dynamical routes of transport in aggregates, shedding light on the many-body effects of the environment as well. We had previously extended this framework to non-Hermitian systems to enable calculation of transport efficiencies and mechanisms in nonequilibrium processes involving a combination of thermal environments and empirically defined losses.[42] However, such a non-Hermitian approach becomes limiting because of nonunitarity of time-evolution, and because it is unable to access various other generic empirical processes. In the current paper, we investigate the possibilities of exploring the dynamics with greater granularity in the presence of multiple pumps and drains affecting the system. We present a generalization of the state-to-state transport analysis which incorporates Lindbladian terms in addition to the effect of thermal solvents, going beyond our own recently developed non-Hermitian state-to-state technique. A crucial aspect of such "mixed" simulations is that the empirical processes are treated under a Markovian approximation using the Lindblad master equation, while the solvent is treated using numerically exact path integrals capturing the non-Markovian memory effects. These empirical processes can either pump or drain the system, or be ones which cause spin decoherence among many others. The Lindblad state-to-state method introduced here allows us to probe the routes of transport in open quantum systems subject to empirical processes described by Lindblad jump operators.

We validated our Lindblad state-to-state method against the non-Hermitian state-to-state analysis for lossy systems. The results from both the methods are consistent. The present method allows us to uncover transport pathways in purely pumped and simultaneously pumped and drained excitonic aggregates, whose dynamics cannot be modeled using non-Hermitian descriptions. While the state-to-state method is directly phrased in terms of diabatic states, we show how to extract monomer-level transport and dynamics information from it. This is especially important for problems where multiple states per monomer can be accessed. We have demonstrated its use in understanding the direct flows, both in the diabatic basis states and between monomers.

In the simultaneously pumped and drained case, we showed the emergence of a steady-state current across the aggregate. Surprisingly, this current is also a function of the aggregate size, even for aggregates of identical monomers. Our Lindblad state-to-state method provides a powerful framework with which one can start to explore these systems. We showed for an excitonic trimer with non-nearest neighbor couplings, that it is possible to separate the unmediated nearest neighbor flow time-scale from the unmediated non-nearest-neighbor flow time scales. Given the richness of these systems, there are many other important parameters to consider and explore. Future work will focus on these and try to deepen our understanding of excitonic currents in transport systems.

One of the hallmarks of the family of state-to-state methods has been the independence of the analysis from the actual method of simulation of the dynamics. This feature is retained in the current work as well. While we have used path integral simulations to generate the dynamics[11,30] here, our method offers the flexibility to use even semiclassical or perturbative approaches. Moreover, using a variety of Lindblad jump operators, one can incorporate processes beyond just pumping and draining and study their effects. This generality makes the Lindblad state-to-state transport analysis method extremely lucrative for unraveling the complexities of the quantum transport in large aggregates subject to empirical processes.

A NON-HERMITIAN HAMILTONIANS AND LINDBLAD JUMP OPERATORS

Consider the Lindblad master equation (eq 8), rewritten here for the sake of convenience:

$$\dot{\rho}(t) = -\frac{i}{\hbar}[\widehat{H}, \rho(t)] + \sum_n \left(L_n \rho(t) L_n^\dagger - \frac{1}{2}\{L_n^\dagger L_n, \rho(t)\} \right) \tag{27}$$

The effect of the Lindbladians on the density matrix $\rho(t)$ above can be split into two parts:[51] the continuous nonunitary dissipation terms $\{L_n^\dagger L_n, \rho(t)\}$ and the quantum jump terms $L_n \rho(t) L_n^\dagger$. The Lindblad master equation is overall trace-preserving and completely positive.

On introducing an effective non-Hermitian Hamiltonian of the form:

$$\widehat{H}_{eff} = \widehat{H} - i \sum_n L_n^\dagger L_n / 2 \tag{28}$$

we note that the master equation in eq 27 can be rewritten in terms of $\hat{H}_{eff}$ as follows:

$$\dot{\rho}(t) = -\frac{i}{\hbar}(\widehat{H}_{eff}\rho(t) - \rho(t)\widehat{H}_{eff}^\dagger) + \sum_n L_n \rho(t) L_n^\dagger \tag{29}$$

If one were to ignore the last term ($\sum_n L_n \rho(t) L_n^\dagger$) in eq 29, the equation becomes the equation of motion for a generic non-Hermitian Hamiltonian. However, as evident, the time evolution no longer satisfies the property of being trace-conserving and completely positive.

This inability of a non-Hermitian Hamiltonian to conserve the trace of the density matrix brings forth several limitations. One such limitation is the fact that there is no commensurate rise in the population of the states into which the system decays. For example, in a two-level system with a non-Hermitian Hamiltonian describing the decay of excited state $|e\rangle$, the decrease in the population of $|e\rangle$ would not lead to any change in the population of the ground state $|g\rangle$. As such, this would introduce spurious effects in absorption spectrum or any other observable requiring trace-conservation.

Another limitation of the non-Hermitian description is its inability to describe pump processes. If one were to use a non-Hermitian Hamiltonian with a positive imaginary part, say, $\hat{H}_{eff} = \hat{H} + i\Gamma/2$ for some diagonal and Hermitian operator Γ, in hopes of simulating a pump (instead of a dissipation/loss always introduced with a negative imaginary part), then one would get $\rho(t) \propto e^{\Gamma t}\rho(0)$ for a purely non-Hermitian time evolution. This leads to an exponential rise of the population of the pumped states, provided they start with a nonzero initial population, which is phenomenologically incorrect. Addition-

https://doi.org/10.1021/acs.jctc.6c00030
J. Chem. Theory Comput. 2026, 22, 3827−3838

ally, the states with zero initial population will never rise on being pumped in such a fashion.

B ALTERNATIVE DERIVATION OF EQ 11

We will demonstrate the absence of the non-Markovian memory kernel in the expression for $\dot{P}_l^H(t)$ given in eq 11. As mentioned, this is a result of the baths coupling with the system through operators that are diagonal in the system basis. To derive this result, we start with a continuum version of the Feynman—Vernon influence functional equation, eq 5:[31]

$$\langle s_N^+|\rho_{sys}(t_f)|s_N^-\rangle = \sum_{s_0^\pm} \int_{s_0^\pm}^{s_N^\pm} \mathcal{D}s^\pm(t)\Big[e^{i(S[s^+(t)]-S[s^-(t)])/\hbar} \times \langle s_0^+|\rho_{sys}(0)|s_0^-\rangle F[s^\pm(t)]\Big] \tag{30}$$

where $s^\pm(t)$ denote the forward and backward paths, S is the classical action along a given path, and $s_N^\pm = s^\pm(t_f)$. The shorthand notation $\int \mathcal{D}s^\pm(t)$ corresponds to the integral over all paths joining the initial state $s_0^\pm$ to the final state $s_N^\pm$. The influence functional $F[s^\pm(t)]$ in the continuous time limit for a bath coupling with the system through an operator that is diagonal in the system basis is given by[31]

$$F[s^\pm(t)] = \exp\Big[-\frac{i}{\hbar}\int_0^{t_f} dt'\Delta s(t')\int_0^{t'} dt''\{\alpha(t'-t'')s^+(t'') - \alpha^*(t'-t'')s^-(t'')\}\Big] \tag{31}$$

where $\Delta s(t) = s^+(t) - s^-(t)$ and $\alpha(t)$ is the bath response function.

Now, we obtain the RDM by solving the path integral in a direct manner numerically. However, the state-to-state transport[21] starts with the time-derivative of the populations as obtained from the time-evolved RDM and the system Hamiltonian. On taking the time derivative of eq 30, one obtains an expression for the rate of change of the RDM matrix elements:

$$\left\langle s_N^+\left|\frac{\partial\rho_{sys}(t_f)}{\partial t}\right|s_N^-\right\rangle = -\frac{i}{\hbar}\langle s_N^+|[\hat{H}_{sys},\rho_{sys}(t)]|s_n^-\rangle + \sum_{s_0^\pm}\int_{s_0^\pm}^{s_N^\pm}\mathcal{D}s^\pm(t)\Big[e^{i(S[s^+(t)]-S[s^-(t)])/\hbar} \times \langle s_0^+|\rho_{sys}(0)|s_0^-\rangle\frac{\partial}{\partial t}F[s^\pm(t)]\Big] \tag{32}$$

where $\partial_t S = -\hat{H}_{sys}$ using the Hamilton-Jacobi theory. The partial derivative of the influence functional can be simplified as

$$\frac{\partial F[s^\pm(t)]}{\partial t} = -\frac{i}{\hbar}\Delta s(t_f)\int_0^{t_f} d\tau(\alpha(t_f-\tau)s^+(\tau) - \alpha^*(t_f-\tau)s^-(\tau)) \times F[s^\pm(t)] \tag{33}$$

Notice that in eq 32, the first term is nothing but the system Liouvillian. Therefore, the second term must correspond to the memory kernel term as arising in the Nakajima-Zwanzig master equation:

$$\dot{\rho}_{sys}(t) = -\frac{i}{\hbar}[\hat{H}_{sys},\rho_{sys}(t)] + \int_0^t \mathcal{K}(\tau)\rho_{sys}(t-\tau)d\tau \tag{34}$$

where $\mathcal{K}(\tau)$ is the non-Markovian memory kernel.

Now, for the case of arriving at the Hamiltonian state-to-state equation, eq 11, we set $s_N^+ = s_N^- = l$ in eq 32. The partial derivative of the influence functional, eq 33, goes to zero for the diagonal flux because $\Delta s(t_f) = 0$. Thus, the memory kernel does not contribute to $\dot{P}_l^H(t)$ and it becomes possible to write eq 11 solely in terms of $\hat{H}_{sys}$ and $\rho_{sys}(t)$.

AUTHOR INFORMATION

Corresponding Author

Amartya Bose − *Department of Chemical Sciences, Tata Institute of Fundamental Research, Mumbai 400005, India;* orcid.org/0000-0003-0685-5096; Email: amartya.bose@gmail.com, amartya.bose@tifr.res.in

Author

Devansh Sharma − *Department of Chemical Sciences, Tata Institute of Fundamental Research, Mumbai 400005, India*

Complete contact information is available at: https://pubs.acs.org/10.1021/acs.jctc.6c00030

Notes

The authors declare no competing financial interest.

REFERENCES

(1) Pullerits, T.; Sundström, V. Photosynthetic Light-Harvesting Pigment-Protein Complexes: Toward Understanding How and Why. *Acc. Chem. Res.* **1996**, *29*, 381−389.

(2) Wu, J.; Liu, F.; Ma, J.; Silbey, R. J.; Cao, J. Efficient Energy Transfer in Light-Harvesting Systems: Quantum-classical Comparison, Flux Network, and Robustness Analysis. *J. Chem. Phys.* **2012**, *137*, 174111.

(3) Ishizaki, A.; Fleming, G. R. Quantum Coherence in Photosynthetic Light Harvesting. *Annual Review of Condensed Matter Physics* **2012**, *3*, 333−361.

(4) Baker, L. A.; Habershon, S. Robustness, Efficiency, and Optimality in the Fenna-Matthews-Olson Photosynthetic Pigment-Protein Complex. *J. Chem. Phys.* **2015**, *143*, 105101.

(5) Ratner, M. A.; Davis, B.; Kemp, M.; Mujica, V.; Roitberg, A.; Yaliraki, S. Molecular Wires: Charge Transport, Mechanisms, and Control. *Ann. N.Y. Acad. Sci.* **1998**, *852*, 22−37.

(6) Mottaghian, S. S.; Biesecker, M.; Bayat, K.; Farrokh Baroughi, M. Unified Electronic Charge Transport Model for Organic Solar Cells. *J. Appl. Phys.* **2013**, *114*, No. 024501.

(7) Makri, N.; Makarov, D. E. Tensor Propagator for Iterative Quantum Time Evolution of Reduced Density Matrices. I. Theory. *J. Chem. Phys.* **1995**, *102*, 4600−4610.

(8) Makri, N.; Makarov, D. E. Tensor Propagator for Iterative Quantum Time Evolution of Reduced Density Matrices. II. Numerical Methodology. *J. Chem. Phys.* **1995**, *102*, 4611−4618.

(9) Tanimura, Y.; Wolynes, P. G. Quantum and Classical Fokker-Planck Equations for a Gaussian-Markovian Noise Bath. *Phys. Rev. A* **1991**, *43*, 4131−4142.

(10) Tanimura, Y. Numerically "Exact" Approach to Open Quantum Dynamics: The Hierarchical Equations of Motion (HEOM). *J. Chem. Phys.* **2020**, *153*, 20901.

(11) Strathearn, A.; Kirton, P.; Kilda, D.; Keeling, J.; Lovett, B. W. Efficient Non-Markovian Quantum Dynamics Using Time-Evolving Matrix Product Operators. *Nat. Commun.* **2018**, *9*, 3322.

(12) Bose, A. Pairwise Connected Tensor Network Representation of Path Integrals. *Phys. Rev. B* **2022**, *105*, No. 024309.

(13) Bose, A.; Walters, P. L. A Multisite Decomposition of the Tensor Network Path Integrals. *J. Chem. Phys.* **2022**, *156*, No. 024101.

(14) Xu, M.; Yan, Y.; Shi, Q.; Ankerhold, J.; Stockburger, J. T. Taming Quantum Noise for Efficient Low Temperature Simulations of Open Quantum Systems. *Phys. Rev. Lett.* **2022**, *129*, No. 230601.
(15) Huo, P.; Coker, D. F. Communication: Partial Linearized Density Matrix Dynamics for Dissipative, Non-Adiabatic Quantum Evolution. *J. Chem. Phys.* **2011**, *135*, 201101.
(16) Mannouch, J. R.; Richardson, J. O. A Partially Linearized Spin-Mapping Approach for Nonadiabatic Dynamics. I. Derivation of the Theory. *J. Chem. Phys.* **2020**, *153*, 194109.
(17) Cotton, S. J.; Miller, W. H. A New Symmetrical Quasi-Classical Model for Electronically Non-Adiabatic Processes: Application to the Case of Weak Non-Adiabatic Coupling. *J. Chem. Phys.* **2016**, *145*, 144108.
(18) Hsieh, C. Y.; Kapral, R. Nonadiabatic Dynamics in Open Quantum-Classical Systems: Forward-backward Trajectory Solution. *J. Chem. Phys.* **2012**, *137*, 22A507.
(19) Hsieh, C. Y.; Kapral, R. Analysis of the Forward-Backward Trajectory Solution for the Mixed Quantum-Classical Liouville Equation. *J. Chem. Phys.* **2013**, *138*, 134110.
(20) Dani, R.; Kundu, S.; Makri, N. Coherence Maps and Flow of Excitation Energy in the Bacterial Light Harvesting Complex 2. *J. Phys. Chem. Lett.* **2023**, *14*, 3835−3843.
(21) Bose, A.; Walters, P. L. Impact of Solvent on State-to-State Population Transport in Multistate Systems Using Coherences. *J. Chem. Theory Comput.* **2023**, *19*, 4828−4836.
(22) Bose, A.; Walters, P. L. Impact of Spatial Inhomogeneity on Excitation Energy Transport in the Fenna−Matthews−Olson Complex. *J. Phys. Chem. B* **2023**, *127*, 7663−7673.
(23) Ishizaki, A.; Fleming, G. R. Unified Treatment of Quantum Coherent and Incoherent Hopping Dynamics in Electronic Energy Transfer: Reduced Hierarchy Equation Approach. *J. Chem. Phys.* **2009**, *130*, 234111.
(24) Ishizaki, A.; Fleming, G. R. Theoretical Examination of Quantum Coherence in a Photosynthetic System at Physiological Temperature. *Proc. Natl. Acad. Sci. U. S. A.* **2009**, *106*, 17255−17260.
(25) Bose, A.; Makri, N. All-Mode Quantum−Classical Path Integral Simulation of Bacteriochlorophyll Dimer Exciton-Vibration Dynamics. *J. Phys. Chem. B* **2020**, *124*, 5028−5038.
(26) Kundu, S.; Dani, R.; Makri, N. B800-to-B850 Relaxation of Excitation Energy in Bacterial Light Harvesting: All-state, All-Mode Path Integral Simulations. *J. Chem. Phys.* **2022**, *157*, No. 015101.
(27) Bose, A.; Walters, P. L. Tensor Network Path Integral Study of Dynamics in B850 LH2 Ring with Atomistically Derived Vibrations. *J. Chem. Theory Comput.* **2022**, *18*, 4095−4108.
(28) Palm, T.; Nalbach, P. Nonperturbative Environmental Influence on Dephasing. *Phys. Rev. A* **2017**, *96*, No. 032105.
(29) Sharma, D.; Bose, A. Non-Hermitian State-to-State Analysis of Transport in Aggregates with Multiple Endpoints. *J. Chem. Theory Comput.* **2025**, *21*, 5858−5866.
(30) Bose, A. Incorporation of Empirical Gain and Loss Mechanisms in Open Quantum Systems through Path Integral Lindblad Dynamics. *J. Phys. Chem. Lett.* **2024**, *15*, 3363−3368.
(31) Feynman, R. P.; Vernon, F. L. The Theory of a General Quantum System Interacting with a Linear Dissipative System. *Annals of Physics* **1963**, *24*, 118−173.
(32) Lindblad, G. On the Generators of Quantum Dynamical Semigroups. *Communications in Mathematical Physics* **1976**, *48*, 119−130.
(33) Gorini, V.; Kossakowski, A.; Sudarshan, E. C. G. Completely Positive Dynamical Semigroups of N-level Systems. *Journal of Mathematical Physics* **1976**, *17*, 821−825.
(34) Mondal, M. E.; Koessler, E. R.; Provazza, J.; Vamivakas, A. N.; Cundiff, S. T.; Krauss, T. D.; Huo, P. Quantum Dynamics Simulations of the 2D Spectroscopy for Exciton Polaritons. *J. Chem. Phys.* **2023**, *159*, No. 094102.
(35) Makri, N.; Thompson, K. Semiclassical influence functionals for quantum systems in anharmonic environments1Presented at the American Physical Society Meeting in Los Angeles, California, USA, March 19, 1998.1. *Chem. Phys. Lett.* **1998**, *291*, 101−109.
(36) Lambert, R.; Makri, N. Quantum-Classical Path Integral. I. Classical Memory and Weak Quantum Nonlocality. *J. Chem. Phys.* **2012**, *137*, 22A552.
(37) Lambert, R.; Makri, N. Quantum-Classical Path Integral. II. Numerical Methodology. *J. Chem. Phys.* **2012**, *137*, 22A553.
(38) Mulvihill, E.; Gao, X.; Liu, Y.; Schubert, A.; Dunietz, B. D.; Geva, E. Combining the Mapping Hamiltonian Linearized Semiclassical Approach with the Generalized Quantum Master Equation to Simulate Electronically Nonadiabatic Molecular Dynamics. *J. Chem. Phys.* **2019**, *151*, 74103.
(39) Mulvihill, E.; Schubert, A.; Sun, X.; Dunietz, B. D.; Geva, E. A Modified Approach for Simulating Electronically Nonadiabatic Dynamics via the Generalized Quantum Master Equation. *J. Chem. Phys.* **2019**, *150*, No. 034101.
(40) Chatterjee, S.; Makri, N. Real-Time Path Integral Methods, Quantum Master Equations, and Classical vs Quantum Memory. *J. Phys. Chem. B* **2019**, *123*, 10470−10482.
(41) Cerrillo, J.; Cao, J. Non-Markovian Dynamical Maps: Numerical Processing of Open Quantum Trajectories. *Phys. Rev. Lett.* **2014**, *112*, No. 110401.
(42) Sharma, D.; Bose, A. Impact of Loss Mechanisms on Linear Spectra of Excitonic and Polaritonic Aggregates. *J. Chem. Theory Comput.* **2024**, *20*, 9522−9532.
(43) Bose, A. QuantumDynamics.Jl: A Modular Approach to Simulations of Dynamics of Open Quantum Systems. *J. Chem. Phys.* **2023**, *158*, 204113.
(44) Sun, K.; Dou, C.; Gelin, M. F.; Zhao, Y. Dynamics of disordered Tavis−Cummings and Holstein−Tavis−Cummings models. *J. Chem. Phys.* **2022**, *156*, No. 024102.
(45) Fitzgerald, J. M.; Rosati, R.; Malic, E. Polariton transport in 2D semiconductors: Phonon-mediated transitions between ballistic, superdiffusive, and exciton-limited regimes. *Sci. Adv.* **2025**, *11*, No. eaea3495.
(46) Krupp, N.; Groenhof, G.; Vendrell, O. Quantum dynamics simulation of exciton-polariton transport. *Nat. Commun.* **2025**, *16*, 5431.
(47) Blackham, L.; Manjalingal, A.; Koshkaki, S. R.; Mandal, A. Microscopic Theory of Polaron-Polariton Dispersion and Propagation. *Nano Lett.* **2025**, *25*, 15874−15882.
(48) Chng, B. X. K.; Mondal, M. E.; Ying, W.; Huo, P. Quantum Dynamics Simulations of Exciton Polariton Transport. *Nano Lett.* **2025**, *25*, 1617−1622.
(49) Bose, A.; Makri, N. Non-Equilibrium Reactive Flux: A Unified Framework for Slow and Fast Reaction Kinetics. *J. Chem. Phys.* **2017**, *147*, 152723.
(50) Dani, R.; Makri, N. Quantum State-to-State Rates for Multistate Processes from Coherences. *J. Phys. Chem. Lett.* **2022**, *13*, 8141−8149.
(51) Wiseman, H.; Milburn, G. *Quantum Measurement and Control*; Cambridge University Press, 2010.

https://doi.org/10.1021/acs.jctc.6c00030
J. Chem. Theory Comput. 2026, 22, 3827−3838